water

MDPI

Article

Response Characteristics and Water Inflow Prediction of Complex Groundwater Systems under High-Intensity Coal Seam Mining Conditions

Zhaolai Hua [1,2], Yao Zhang [1,*], Shihao Meng [1], Lu Wang [1,2], Xuejun Wang [3], Yang Lv [1,2], Jinming Li [2], Shaofeng Ren [2], Han Bao [1], Zhihao Zhang [1], Linger Zhao [1] and Yifan Zeng [1,*]

[1] Nation Engineering Research Center of Coal Mine Water Hazard Controlling, China University of Mining and Technology, Beijing 100083, China; huazhaolai110@163.com (Z.H.); meng_shihao@outlook.com (S.M.)
[2] Shaanxi Shanmei Caojiatan Mining Co., Ltd., Yulin 719000, China; sqt2100203063@student.cumtb.edu.cn (J.L.)
[3] Tangshan Kailuan Construction (Group) Co., Ltd., Tangshan 063000, China
* Correspondence: zqt2100203105@student.cumtb.edu.cn (Y.Z.); zengyf@cumtb.edu.cn (Y.Z.)

Abstract: With the gradual improvement in coal mining efficiency, the disturbance of groundwater systems caused by high-intensity mining also increases, leading to challenges in maintaining mine safety and protecting water resources in mining areas. How to accurately describe the dynamic changes in the groundwater system under mining and quantitatively predict mine water inflow are currently major problems to be addressed. Based on a full analysis of the response characteristics of a groundwater system to the extraction disturbance, this paper presents a new method to establish a mine hydrogeological conceptual model that can accurately represent the water inrush process. The unstructured-grid package of MODFLOW is used to accurately characterize the formation structure and finally make accurate water inflow predictions. Taking the Caojiatan coal mine in Shaanxi Province, China, as an example, a numerical model of unstructured water inflow is established, and the changes in the water inflow source and intensity are quantitatively evaluated. Compared with the traditional water inflow prediction method, the prediction accuracy of the new model is improved by 12–17%, which is achieved by detailing the response of the complex groundwater system under high-intensity mining conditions. The method presented in this paper has great significance and applicatory value for obtaining a comprehensive understanding of the disturbance characteristics of human underground engineering activities (e.g., coal mining) on groundwater systems, as well as accurately predicting water inflow.

Keywords: coal mine water hazard; MODFLOW; non-structural mesh; mine hydrogeology

Citation: Hua, Z.; Zhang, Y.; Meng, S.; Wang, L.; Wang, X.; Lv, Y.; Li, J.; Ren, S.; Bao, H.; Zhang, Z.; et al. Response Characteristics and Water Inflow Prediction of Complex Groundwater Systems under High-Intensity Coal Seam Mining Conditions. *Water* **2023**, *15*, 3376. https://doi.org/10.3390/w15193376

Academic Editor: Yeshuang Xu

Received: 31 August 2023
Revised: 18 September 2023
Accepted: 21 September 2023
Published: 26 September 2023

1. Introduction

In recent years, engineering activities have no longer been limited to the Earth's surface and have gradually extended underground. However, the development of underground engineering has caused serious damage to geological structures and groundwater systems. With the increase in human activity, it has become crucial to evaluate the impact of underground engineering on the environment and their interaction. Mining activities are common, and long-term, high-intensity coal mining has become one of the most typical underground engineering activities [1]. Water inrush in mines is a frequent occurrence during the mining process, posing serious threats to the safety of miners and causing significant economic losses [2]. Moreover, it also seriously damages groundwater systems [3,4]. Weather and drainage wells are the main driving factors for the impact of general underground engineering activities on groundwater systems, whereas those of coal mining are mainly water inflow and overlying strata damage caused by mining activities. Therefore, establishing a conceptual model under high-strength coal mining is of great importance to analyze how mining disturbs groundwater systems [5].

Currently, there are many studies on how mining disturbs groundwater systems, which mainly focus on the circulation, chemical characteristics, and evolution of the groundwater system [6,7]. Regarding the water inrush problems, Zeng et al. [8–10] achieved a series of research results on the water-richness in the roof, the identification of water sources for water inrushes, and mine water drainage. Ta et al. developed a numerical groundwater model, based on a conceptual hydrogeologic model of the Thach Khe iron ore mine and its surrounding area in Vietnam, and evaluated various scenarios to estimate groundwater ingress at different stages of the mine life [11]. Duan et al. [12] studied the tracing of groundwater by environmental isotopes and artificial radioisotopes, providing a basis for the application of isotopes in water cycling, and evaluated the impact of different factors. Under the dual carbon background, Wu et al. [13–15] proposed a theory of positive synergistic and coordinated coal-water-heat co-mining, providing an approach for the green and coordinated utilization of groundwater, coal resources, and geothermal resources. In recent years, many scholars have also made significant efforts toward the precise prediction of mine water inflow [16,17]. The main methods for predicting water inflow include the virtual large-diameter well method [18,19], analytical methods [20,21], the hydrogeological analogy method [22], and numerical simulation methods [23,24]. Unfortunately, these traditional methods often cannot accurately describe the response characteristics of groundwater systems under the conditions of high-intensity coal mining [25–27]. Therefore, establishing a hydrogeological conceptual mine model is critical to studying groundwater systems.

Based on comprehensive investigations of the Caojiatan coal mine in Shaanxi, China, this study summarizes a set of methods for constructing a model that accurately reflects the process of water inflow. Combined with numerical simulation, it accurately characterizes the process and intensity of water inflow at the working face. Our results have reference value for studying the disturbance of underground engineering activities on groundwater systems.

2. Study Area

The Caojiatan coal mine is located in the northern part of Yulin City, Shaanxi Province, China (Figure 1). It lies on the northeastern edge of the Ordos Plateau, adjacent to the southeastern edge of the Mu Us Desert, and features sand dunes, wind-blown sand plains, and loess landforms. The climate is characterized by fluctuating temperatures throughout the year, low rainfall, and high evaporation, and precipitation is extremely unevenly distributed throughout the year. The mining area belongs to the Tuwei River Basin and the Yuxi River Basin. There is a north–south watershed in the middle of the study area, which divides the confined aquifer into two relatively independent hydrogeological units, east and west.

The stratigraphic layers in the study area, from top to bottom, are as follows: the Quaternary Upper Member Salarwusu Formation (Q_3s), the Quaternary Middle Member Lishi Formation (Q_2l), the Neogene Upper Member Baode Formation (N_2b), the Jurassic Middle Member Anding Formation (J_2a), the Jurassic Middle Member Zhiluo Formation (J_2z), the Jurassic Middle Member Yan'an Formation (J_2y), and the coal seam (Figure 2).

The Salawusu Formation (Q_3s) is widely distributed across the study area, with only a partial absence observed at the watershed. The sand layer is characterized by significant thickness, high permeability, and a high capacity to be recharged from rainfall. Groundwater is moderately abundant in this formation, and the overall direction of groundwater flow is from northeast to southwest.

The Lishi Formation (Q_2l) is distributed throughout the western flank of the study area. At the watershed, the layer partially emerges at the surface. The lithology of this layer is heterogeneous, mainly consisting of sandy loam and silt, and it exhibits good vertical permeability.

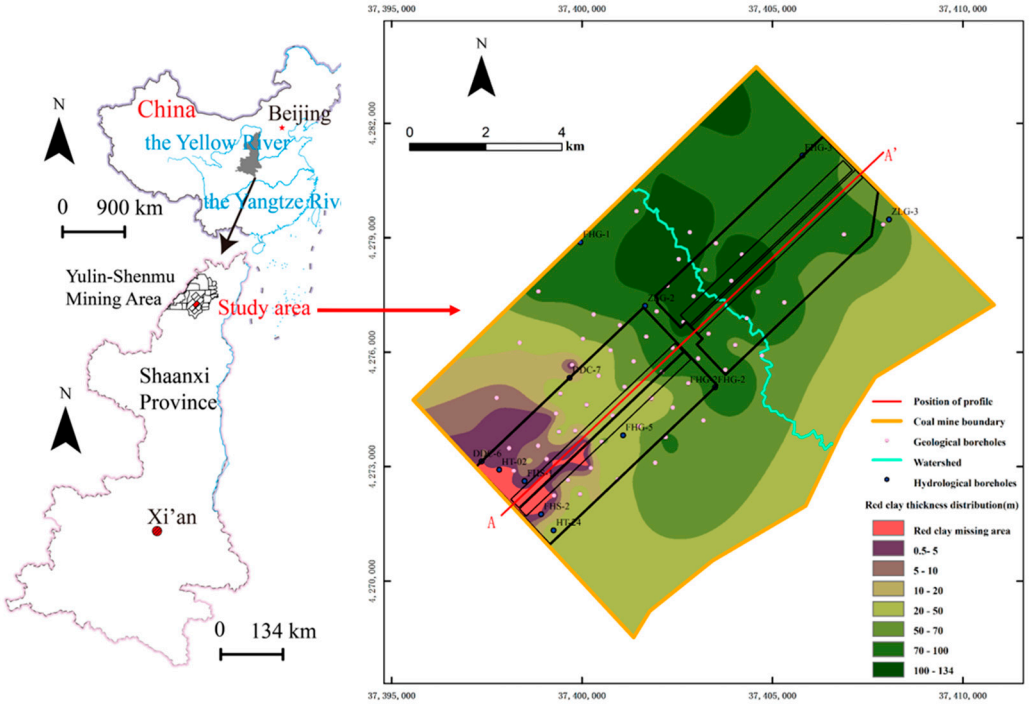

Figure 1. Location of Caojiatan well field and distribution map of laterite aquifer.

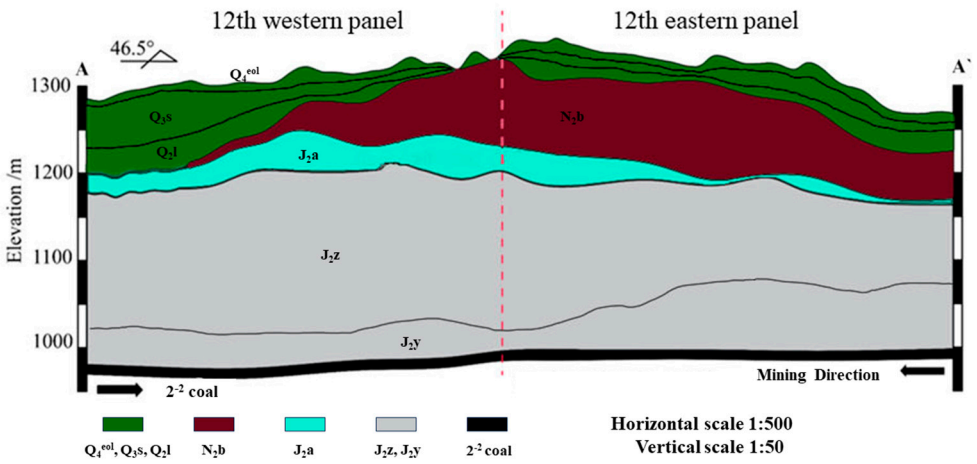

Figure 2. A-A′ typical profile view.

The Baode Formation (N_2b) becomes thinner from the watershed toward the west and southwest directions. The lithology mainly consists of reddish-brown clay and sub-clay. The soil gradually decreases in the western wing of the mining area, and there is some red soil erosion loss at the western boundary, with a cumulative area of 1.31 km^2. The distribution of the red clay layer and the hydrological parameters of the strata were mainly obtained by collecting geological and hydrological borehole data from the study area. The boreholes are shown in Figure 1.

The Anding Formation (J_2a) is distributed throughout the western part of the oilfield, with a relatively small abundance of groundwater.

The Zhiluo Formation (J_2z) shows no weathering at the top and mainly consists of blue-gray mudstone and siltstone. Its fissures are poorly developed, resulting in a low overall abundance of groundwater.

The Yanan Formation (J_2y) mainly consists of medium- to fine-grained sandstone with mud or calcareous cementation. Its fissures have poor connectivity, leading to a low abundance of groundwater. The thickness of 2^{-2} coal in the study area is 11.72~12.7 m.

3. Study Methods

We used the mine hydrogeological conceptual modeling method, the traditional hydrogeological conceptual modeling method, the hydrogeological analog method, and the Grey Model (1,1) in this study.

3.1. Mine Hydrogeological Conceptual Model

The mine conceptual hydrogeological model has different driving forces compared to traditional hydrogeological models: those of the latter are mainly weather and drainage wells, whereas that of the former is overlying strata damage caused by mining activities and water inflow. At the same time, because mining activities have more intense characteristics, the mine hydrogeological conceptual model has features of instantaneous change in addition to static simulations, which are typical of traditional hydrogeological models.

Specifically, to establish the mine hydrogeological conceptual model, the following three aspects need to be addressed:

1. The geological characteristics of the mining area must be analyzed and studied, including geological structure, rock type, and stratigraphy. Through the investigation of geological characteristics, the lithological characteristics, spatial structure, water-richness, permeability, and stratigraphic structure of each aquifer or aquitard in the research area can be determined. This is the geological basis for establishing a hydrogeological conceptual model for mining areas.
2. The development height of the water-bearing fractured zone, as well as the water inflow intensity and whether there is leaking recharge, must be analyzed and studied in order to understand where the water comes from and where it goes. After coal mining, the underground area will suffer mining damage; at this time, the thickness of the bedrock of the roof of the mining working face and the development height of the water-bearing fractured zone determine the range of water inflow channels. An empirical formula [28] for determining the height of the water-bearing fractured zone is given as follows:

$$H_f = 20M + 10 \quad (1)$$

   where H_f is the height of the water-conducting fracture zone (L) and M is the thickness of the coal seam (L).
3. The chemical characteristics of the mine water must be analyzed and studied, including the pH value, electrical conductivity, hardness, and the contents of anions and cations, in order to identify the source of water inflows. By considering the characteristics of mine water inflow, we can determine the recharge impact of the overlying aquifers on the mine water inflow.

In summary, establishing the mine conceptual hydrogeological model involves comprehensive analyses of the hydrogeological characteristics, water chemistry, water inflow sources, height of water-conductive fracture zones, and water inflow intensity. This method provides a theoretical foundation for studying the changing characteristics of underground water systems and predicting water inflow in mines.

3.2. Numerical Simulation Method

The numerical simulation method uses the MODFLOW-USG (Unstructured Grid) version released by the United States Geological Survey in 2013. The version supports various structured and unstructured grid types, and its flexibility in refining the density of unstructured grids can achieve precise characterization of the grid in the working face.

The governing equation for groundwater flow and boundary control is as follows:

$$\begin{cases} \frac{\partial}{\partial x}\left(K_L\frac{\partial h}{\partial x}\right)+\frac{\partial}{\partial y}\left(K_L\frac{\partial h}{\partial y}\right)+\frac{\partial}{\partial z}\left(K_z\frac{\partial h}{\partial z}\right)+\varepsilon=0, x,y,z\in\Omega_1 \\ \frac{\partial}{\partial x}\left(K_L(h-h_b)\frac{\partial h}{\partial x}\right)+\frac{\partial}{\partial y}\left(K_L(h-h_b)\frac{\partial h}{\partial y}\right)+K_z\frac{\partial}{\partial z}\left(\frac{\partial h}{\partial z}\right)+\varepsilon=0, x,y,z\in\Omega_2 \\ h(x,y,z)=h_0, x,y,z\in\Omega \\ K_{\vec{\gamma}}\frac{\partial h}{\partial \vec{\gamma}}|\Gamma_1=q, x,y,z\in\Gamma_1 \\ K_{\vec{\gamma}}\frac{\partial h}{\partial \vec{\gamma}}|\Gamma_2=\frac{k}{m}(h_2-h), x,y,z\in\Gamma_2 \end{cases}, \quad (2)$$

$$\begin{cases} \frac{\partial}{\partial x}\left(K_L\frac{\partial h}{\partial x}\right)+\frac{\partial}{\partial y}\left(K_L\frac{\partial h}{\partial y}\right)+\frac{\partial}{\partial z}\left(K_z\frac{\partial h}{\partial z}\right)+\varepsilon=S\frac{\partial h}{\partial t}, x,y,z\in\Omega_1, t\geq 0 \\ \frac{\partial}{\partial x}\left(K_L(h-h_b)\frac{\partial h}{\partial x}\right)+\frac{\partial}{\partial y}\left(K_L(h-h_b)\frac{\partial h}{\partial y}\right)+\frac{\partial}{\partial z}\left(K_z\frac{\partial h}{\partial z}\right)+\varepsilon=u\frac{\partial h}{\partial t}, x,y,z\in\Omega_2, t\geq 0 \\ h(x,y,z,t)|_{t=0}, x,y,z\in\Omega \\ K_{\vec{\gamma}}\frac{\partial h}{\partial \vec{\gamma}}|\Gamma_1=q, x,y,z\in\Gamma_1, t\geq 0 \\ K_{\vec{\gamma}}\frac{\partial h}{\partial \vec{\gamma}}|\Gamma_2=\frac{k}{m}(h_2-h), x,y,z\in\Gamma_2, t\geq 0 \end{cases}, \quad (3)$$

where Equation (2) is the steady flow control equation and Equation (3) is the unsteady flow control equation. The symbols used in the equation are defined as follows:

- Ω—Domain of the porous medium;
- Ω_1—Groundwater aquifer flow zone;
- Ω_2—Confined aquifer flow region;
- Γ_1—Lateral and bottom boundaries of Ω;
- h—Head of the aquifer (L);
- h_b—Elevation of the bottom of the confined aquifer;
- K_L, K_z—Coefficients of horizontal and vertical hydraulic conductivity (LT^{-1});
- ε—Source/sink term of the aquifer (T^{-1});
- S—Specific storage coefficient of the aquifer (L^{-1});
- μ—Specific storage of the confined aquifer;
- h_0—Initial value of the head of the aquifer (L);
- h_1—Initial groundwater level calculated using the steady-state flow model (L);
- K_n—Coefficient of permeability in the direction of the normal of the boundary surface (LT^{-1});
- q—Flow rate in Γ_1, positive for inflow and negative for outflow; q is zero for impermeable boundaries (LT^{-1});
- γ—Normal direction to the boundary surface;
- Γ_2—Generalized hydraulic head boundary of the flow region;
- h_2—Specified hydraulic head outside the Γ_2 boundary;
- k—Hydraulic conductivity of the aquifer between the boundary at Γ_2 and the specified hydraulic head position at h_2;
- m—Thickness of the aquifer between the boundary at Γ_2 and the specified hydraulic head position at h_2.

The goaf is generalized as a drain boundary by using the MODFLOW module in the Groundwater Modeling System [29–34]. The principle of The Drain (DRN) Package is as follows:

$$Q_{out}=\begin{cases} CD\left(h_{i,j,k}-HD\right) & h_{i,j,k}>HD \\ Q_{out}=0 & h_{i,j,k}\leq HD \end{cases}, \quad (4)$$

where Q_{out} is the flow from the aquifer into the drain (L^3T^{-1}), CD is the drain conductance (L^2T^{-1}), HD is the drain elevation (L), and $h_{i,j,k}$ is the head in the cell containing the drain (L).

The following formula is used for fitting the error (Equation (5)):

$$\delta = \frac{\sqrt{\sum_{k=1}^{n}\left(h_k - h'_k\right)^2}}{n\Delta h} \times 100\%, \tag{5}$$

where δ is the groundwater level fitting error (%), n is the number of stress periods in the model, Δh is the maximum measured water level variation during the operation period (L), h_k is the measured groundwater level during stress period k (L), and h'_k is the simulated groundwater level during stress period k (L).

3.3. Grey Model (1,1)

The grey theory [35,36] is a mathematical method used to deal with problems involving incomplete data and high uncertainty. It consists of the grey system theory and grey prediction methods, aiming to reveal the inherent patterns of a system through the analysis and prediction of incomplete data. The GM(1,1), or grey model, which is a single-variable time series prediction model based on grey system theory, generates new data sequences by performing first-order accumulations on the original data, and then constructs differential equation models using these new data sequences to achieve the time series prediction [37]. The steps are as follows:

- Establish a first-order accumulation to generate a sequence of numbers.

  Suppose the non-negative original sequence is $x^{(0)}$:

$$x^{(0)} = \left(x^{(0)}(1), x^{(0)}(2), x^{(0)}(3), \ldots, x^{(0)}(n)\right), x^{(0)}(k) > 0, k = 1, 2, \ldots, n. \tag{6}$$

  The accumulation sequence $x^{(1)}$ of $x^{(0)}$ is

$$x^{(1)} = \left(x^{(1)}(1), x^{(1)}(2), x^{(1)}(3), \ldots, x^{(1)}(n)\right), \tag{7}$$

$$x^{(1)}(k) = \sum_{i=1}^{k} x^{(0)}(i). \tag{8}$$

- The assumed first-order model for generating the sequence is

$$\frac{dx^{(1)}}{dt} + ax^{(1)} = b \qquad t \in \underline{[0, \infty]}. \tag{9}$$

- The dynamic model of the differential equation is given by

$$z^{(1)}(k) = 0.5x^{(1)}(k) + 0.5x^{(1)}(k-1), \tag{10}$$

$$x^{(0)}(k) + az^{(1)}(k) = b, \tag{11}$$

- The least-squares method is used to find the parameters a and b:

$$B = \begin{Bmatrix} -\frac{1}{2}\left[x^{(1)}(1) + x^{(1)}(2)\right], & 1 \\ -\frac{1}{2}\left[x^{(1)}(2) + x^{(1)}(3)\right], & 1 \\ \cdots & \\ -\frac{1}{2}\left[x^{(1)}(n-1) + x^{(1)}(n)\right], & 1 \end{Bmatrix}, \tag{12}$$

$$y_n = \left[x^{(0)}(2), x^{(0)}(3), \ldots, x^{(0)}(n)\right]^T, \tag{13}$$

  Identification of parameters a and b:

$$\beta = \begin{bmatrix} a \\ b \end{bmatrix} \tag{14}$$

$$\beta = \left(B^T B\right)^{-1} B^T y_n \tag{15}$$

- Solving:

$$\hat{x}^{(1)}(k+1) = \left(x^{(0)}(1) - \frac{b}{a}\right)e^{-ak} + \frac{b}{a},\ k = 1,\ 2,\ \cdots,\ n-1 \tag{16}$$

3.4. Hydrogeological Analog Method

The hydrogeological analog method is a groundwater exploration method that uses accumulated data from mining wells with similar geological and hydrogeological conditions, and mining methods to predict the water inflow of the designed mining well. The hydrogeological analog method mainly relies on qualitative analysis rather than quantitative data analysis. The following formula is used for calculations [38]:

$$Q = Q_0(\sqrt[c]{\frac{F}{F_0}})(\sqrt[d]{\frac{S}{S_0}}), \tag{17}$$

where Q is the water inflow of the mine (L^3T^{-1}), Q_0 is the water inflow of the production mine (L^3T^{-1}), F is the mining area (L^2), F_0 is the actual mining area of the production mine (L^2), S is the drawdown of the water level (L), S_0 is the drawdown of the water level in the production mine (m), c = 1, and d = 2.

3.5. Traditional Hydrogeological Conceptual Model

The traditional hydrogeological conceptual model involves generalizing the boundary properties, internal structure, permeability, hydraulic characteristics, and recharge/discharge conditions of the aquifer into mathematical and physical forms. This process aims to quantify the hydrogeological elements and achieve an accurate numerical simulation. The main aspects of the traditional hydrogeological conceptual model include the following:

- Determining the model domain: The model domain refers to the spatial extent within which the hydrogeological processes will be simulated. It is determined based on the research objectives, the characteristics of the study area, and available observational data.
- Generalization of the aquifer (Aquitard): In numerical modeling, it is common practice to group aquifers (and aquitards) with similar hydraulic properties and close hydraulic connections into a unified aquifer (or aquifer system).
- Generalization of boundary conditions: The model boundaries consist of horizontal boundaries and vertical boundaries. The generalization of boundaries should accurately represent the hydrogeological prototype of the study area, and the generalized boundary conditions should reflect the characteristics of the groundwater flow field in the study area. In the generalization process, natural boundaries should be utilized as much as possible to maintain the representativeness of the model. Natural boundaries refer to physical features such as rivers, lakes, or impermeable formations that naturally limit the flow of groundwater. When determining the properties of artificial boundaries, it is important to consider any relevant adverse factors that may affect the groundwater flow field (e.g., pumping wells, hydraulic barriers, or other anthropogenic influences).

4. Results and Discussion

4.1. Water Inflow Prediction Using Numerical Simulation Method

4.1.1. Establishment of Mine Hydrogeological Conceptual Model

The simulation scope of this study is the western area of the Caojiatan coal mine. The surface topography of the 122107 working face mainly comprises crescent-shaped sand

dunes with some vegetation. The terrain gradually decreases from the southwest to the northeast. No major faults, igneous rocks, or folding structures are found within the area.

The first step to establish the mine hydrogeological conceptual model of the study area is to analyze the spatial distribution, lithological characteristics, and hydrological properties of the aquifers (aquitards) within the Caotan 122107 working face field.

Based on the hydrological characteristics and hydraulic connections of each aquifer, we classify layers with similar properties into an aquifer group. Therefore, the model is divided into five layers (Figure 3) from top to bottom. The first layer consists of Quaternary porous aquifers, mainly those of the Salawusu Formation aquifer and Lishi Formation. The second layer consists of red clay aquitards of the Baode Formation. The third layer consists of weathered bedrock aquifers. The fourth layer consists of bedrock aquifers, primarily those of the Yanan Formation and Zhiluo Formation. The fifth layer is the 2^{-2} coal seam.

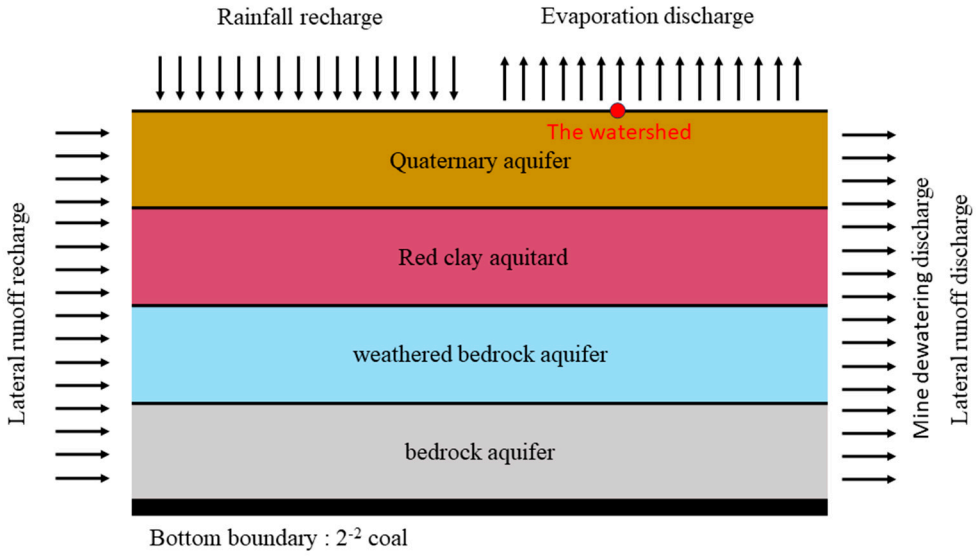

Figure 3. Conceptual hydrogeological model.

The second step to establish the mine hydrogeological conceptual model of the study area is to analyze the overlying strata damage after coal mining, predict the development height of the water-conducting fracture zone, and determine the range of water inflow channels.

Formula (1) is used as an empirical formula to determine the development height of water-conducting fractured zones, and the mining height is 11 m. After comparing the results of drilling fluid loss measurements, borehole color TV detection [39], and core data, we find that the normal bedrock layer has a thickness ranging from 167.25 to 254.96 m above the 122107 working face, and the height of the developed water-conducting fracture zone is 183.00 m, most of which has penetrated the weathered rock aquifer and some of which has reached the bottom of the Salawusu Formation aquifer in the red soil extinction area. By analyzing the distribution of the water-conducting fracture zone and the thickness of the bedrock, and calculating the difference between the two, we determined the influence range of the water-conducting fracture zone. On the west side of the 122107 workface, the central area is more affected, and the southern area of the west side is stronger than the northern area.

In the red soil extinction area (Figure 1), there is a possibility of leakage recharge from the Salawusu Formation aquifer to the weathered bedrock. Simultaneously, the water-conducting fracture zone may develop to the bottom of the Salawusu Formation aquifer in the area with thin red soil, leading to a sudden increase in water inflow. In most areas of the working face, the maximum height of the water-conducting fracture zone extends into the weathered bedrock (Figure 4). Therefore, the aquifers of the Zhiluo Formation and the Yanan Formation supply water directly to the 2^{-2} coal seam.

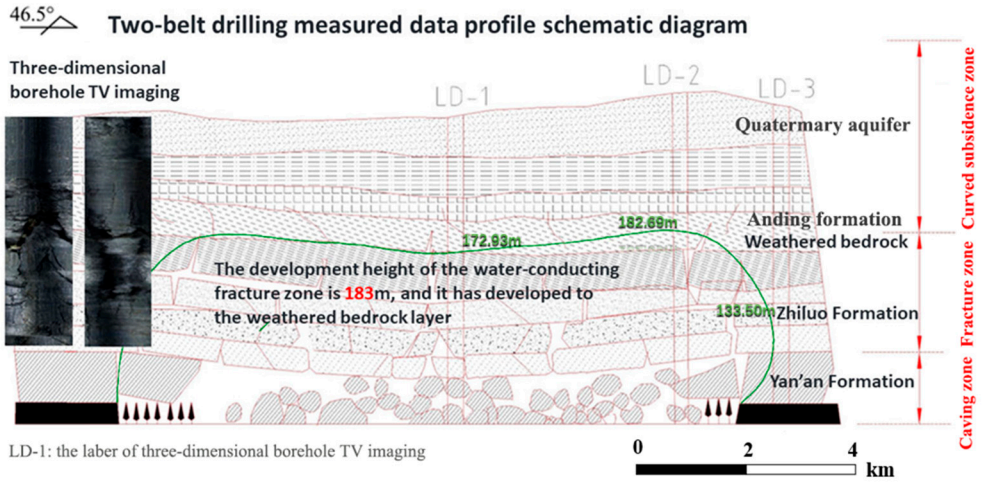

Figure 4. Measured profile of the height of the water-bearing fracture zone in the inclined direction of 122107 working face (LD-1, LD-2).

The third step to establish the mine hydrogeological conceptual model of the study area involves analyzing the source of mine water inflow and the variation in water inflow intensity with mining time to determine the water source and intensity characteristics of mine water inflow at different stages. We use a random forest model [13] with 13 physicochemical indicators, including total dissolved solids (TDS), total hardness (TH), pH, total alkalinity (TA), K^+, N_a^+, Ca_2^+, Mg_2^+, Cl^-, SO_4^{2-}, HCO_3^-, CO_3^{2-}, and NO_3^- to perform water chemistry analysis. The results are shown in Table 1 (higher scores indicate a higher probability of originating from this aquifer), which indicates that during the initial stage of mining at the 122109 working face, the main source of water inflow is from the weathered bedrock aquifer, whereas after stabilization, the water is mainly from the Quaternary aquifer.

Table 1. Identification results of eye cutting water source at 122109 working face.

Time	Score			Results
	Quaternary Water	Weathered Bedrock Water	Bedrock Water	
February 2020	0.2033	0.4533	0.3433	Weathered bedrock water
February 2021	0.4200	0.2367	0.3433	Quaternary water

The intensity of mine water inflow is mainly related to several factors: the aquifer productivity of the overlying strata above the coal seam being extracted, the thickness of the bedrock above the coal seam, the degree of communication between water-conducting fracture zones and various aquifers, atmospheric precipitation, the aquitard properties of the post-mining red soil layer, and the mining method and intensity. As mining progresses, the amount of water inflow continues to increase, stabilizing at 650 m^3/h after mining is completed (Figure 5).

The analysis above shows that the water inflow mainly is from the static storage and leaking replenishment of the weathered rock aquifer during the mining, and there is also lateral groundwater recharge from the Quaternary aquifer. After mining, the stable water inflow is from lateral replenishment of the weathered rock aquifer and the Quaternary aquifer.

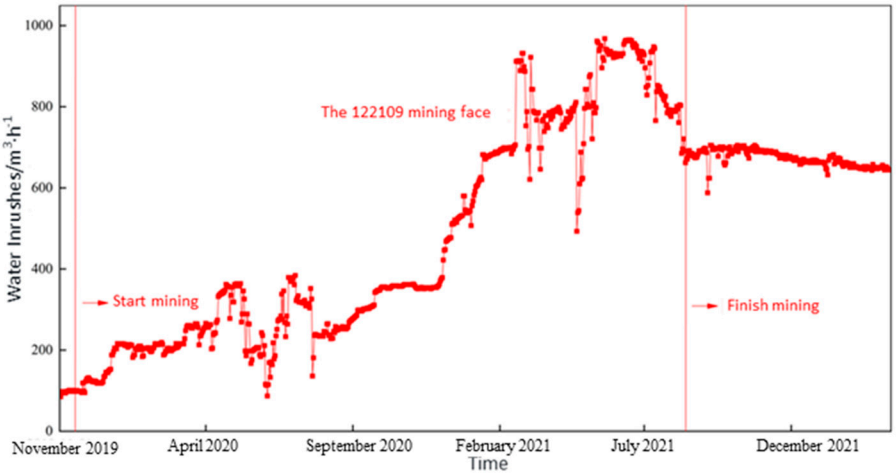

Figure 5. Distribution of water inflow curve for the 122109working face (measured data from the working face).

4.1.2. Numerical Simulation Model

The study area is vertically divided into five layers. By collecting borehole and elevation data, a three-dimensional structure of the model (Figure 6a) and the hydrogeological cross-section map (Figure 6b) are generated using the Kriging interpolation method [40].

The model uses unstructured grids to partition each layer. In the horizontal direction, the study area is set as a grid of 200 m × 200 m, the east and west wings of the 12-panel area are set as a grid of 100 m × 100 m, and the 122107 working face is set as a grid of 50 m × 50 m. There is a certain range of missing stratigraphic layers in the red soil aquitard of the second layer in the west wing of the 12-panel area (Figure 7), and other layers are normally distributed.

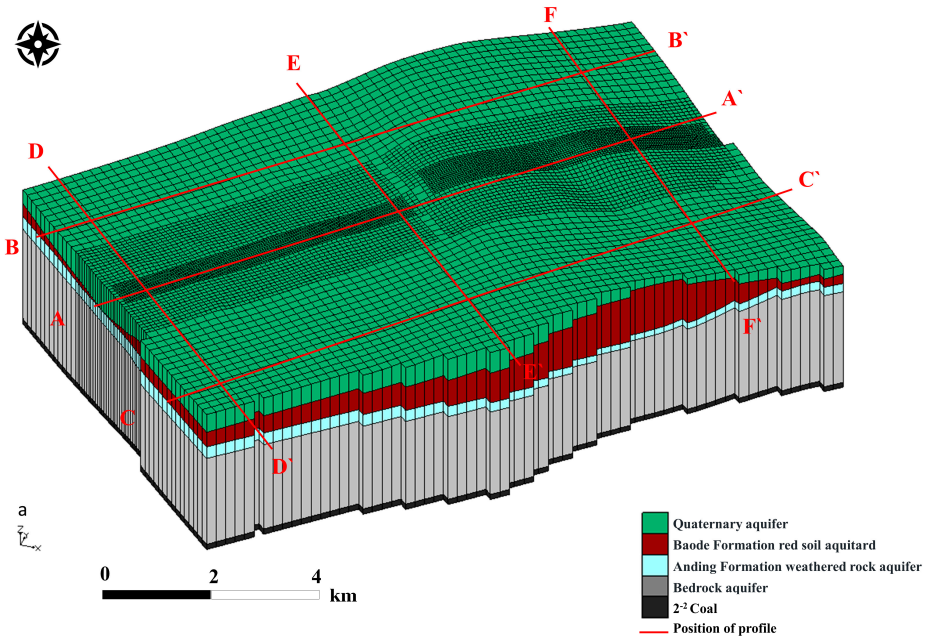

Figure 6. *Cont.*

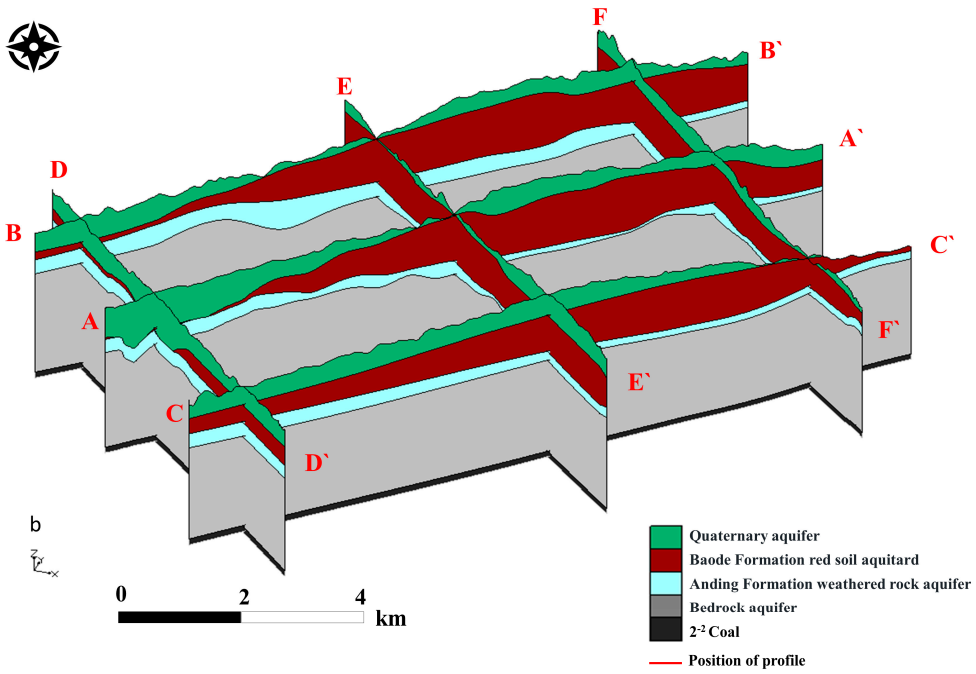

Figure 6. Schematic diagram of the hydrogeological conceptual model: three-dimensional structural model; hydrogeological joint profile. (**a**) three-dimensional structure of the model and (**b**) the hydrogeological cross-section map.

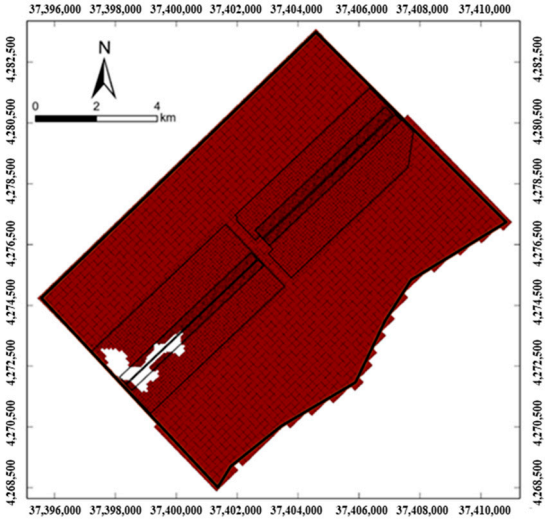

Figure 7. Schematic diagram of unstructured grid division of the second layer of laterite aquifer.

Based on the actual hydrogeological conditions, the watershed position of the first layer is set as the aquitard boundary. Other non-natural boundaries are set as general head boundaries in the horizontal direction, and the free water surface of the upper aquifer is set as the upper boundary of the model in the vertical direction. The bottom of the geological layer in the lower part of the model is set as the aquitard boundary. The goaf of the coal seam is generalized as a drain boundary, and the hydrogeological parameters of each aquifer or aquitard are obtained from pumping test data of the hydrological boreholes.

The study area is mainly covered by Quaternary loose sand layers, and atmospheric rainfall is considered an indirect source of water for the working face. The main water sources and sinks are rainfall and evaporation, respectively. The data are obtained from monthly average rainfall and average evaporation data (Figure 8). The amount of water inflow is determined and verified by balancing the flow into and out of the drainage ditch.

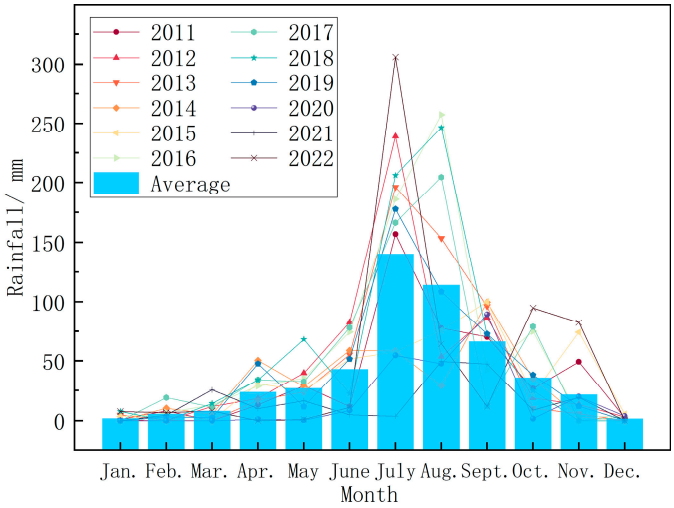

Figure 8. Composite monthly average rainfall map of the study area (these data are derived from the local meteorological services).

In this simulation, a steady-state flow model is established after the 122109 working face is mined. Then, based on the initial flow field, the numerical simulation model is used to investigate the changes in groundwater systems, as fitted with the observed water level data and measured water inflow. The stable flow field within the 12th western panel is depicted in Figure 9.

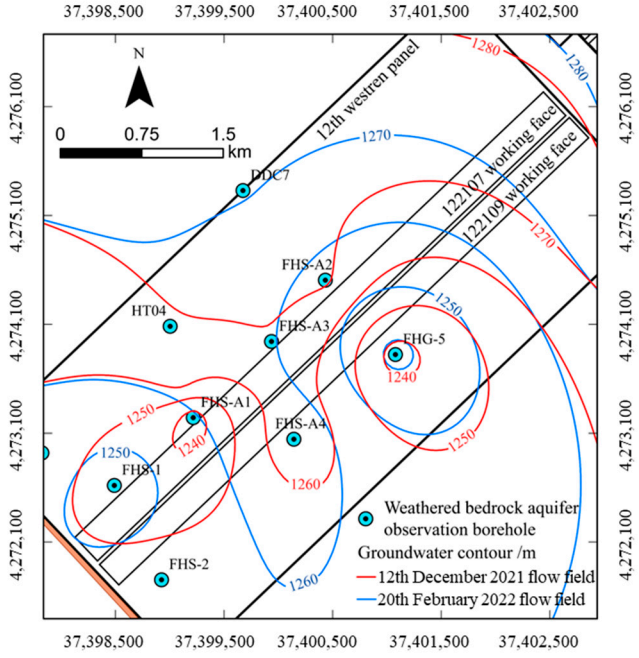

Figure 9. Distribution of the stable flow field in the weathered bedrock aquifer of the 12th western panel.

The simulation period of the model is from 1 February 2022 to 31 January 2027. The identification and validation of the model are divided into two parts: stable flow and unsteady flow. In stable flow, a single stable landing funnel ending with the cessation of 122109 workface mining is finally formed by adjusting the boundary conditions and hydrogeological parameters. These flow data are used as the initial flow field of unsteady flow for the simulation of 122107 workface mining. We add pumping wells to simulate the actual pumping of the FHS-1 and FHS-2 wells. By adjusting the parameters, we

aim to calibrate the model while fitting the simulated values of the pumping wells to actual values.

In this paper, we reduce the mining damage process by adjusting the permeability coefficient of the overlying rock of the working face, which is a constant due to the limitation of the software and cannot simulate the dynamic change in the coefficient with the mining process. Therefore, we can only obtain the magnitude of water influx within a fixed mining length by equalizing the groundwater over a period of time. The final parameters and their zoning for the Quaternary and weathered bedrock aquifers are shown in Figures 10 and 11, and Table 2, respectively.

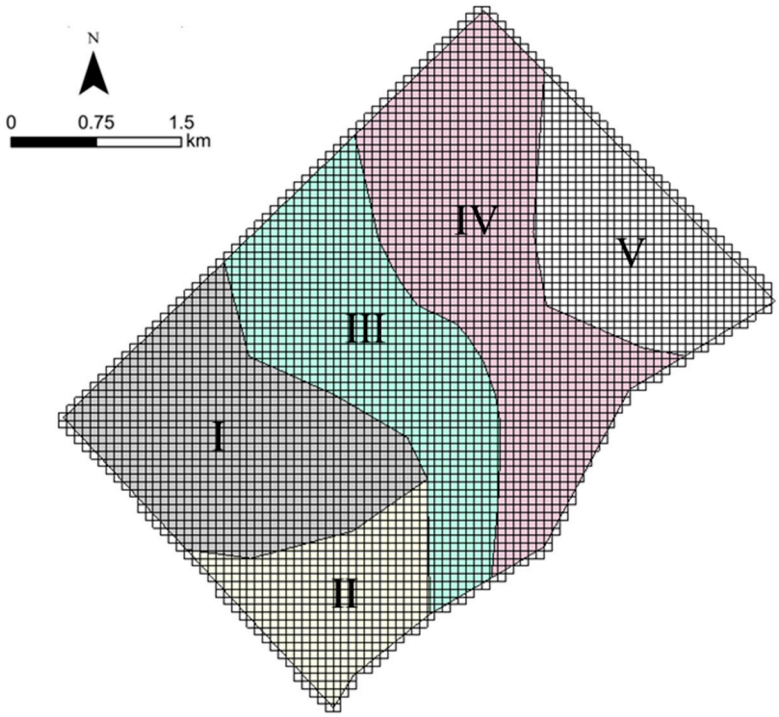

Figure 10. Aquifer parameter zoning (Quaternary aquifer).

The fitting is performed for a duration of 48 h (Figures 12 and 13).

The calculated results suggest that the groundwater level fitting errors for boreholes FHS-1 and FHS-2 are 2.37% and 2.03%, respectively, both of which are less than 5%. These results indicate that the fitting is good, and the numerical model is consistent with the actual situation. Therefore, the numerical model can be used to predict the water inflow.

Based on the model, the permeability coefficient of the rock formation above the 122107 working face is adjusted, and the unsteady flow simulation is performed. The simulation results show that the normal water inflow for the 122107 working face is approximately 826 m^3/h, and the maximum water inflow, calculated as 1.25 times the normal water inflow, is approximately 1032 m^3/h. This value is a safety factor for surge prediction and increases as the mine becomes more water-rich. This safety factor is applied to account for uncertainties and potential variations in the actual groundwater inflow compared to the predicted values. It helps to ensure that the mining operations are adequately prepared to manage and control water inflows for safe and efficient mining activities.

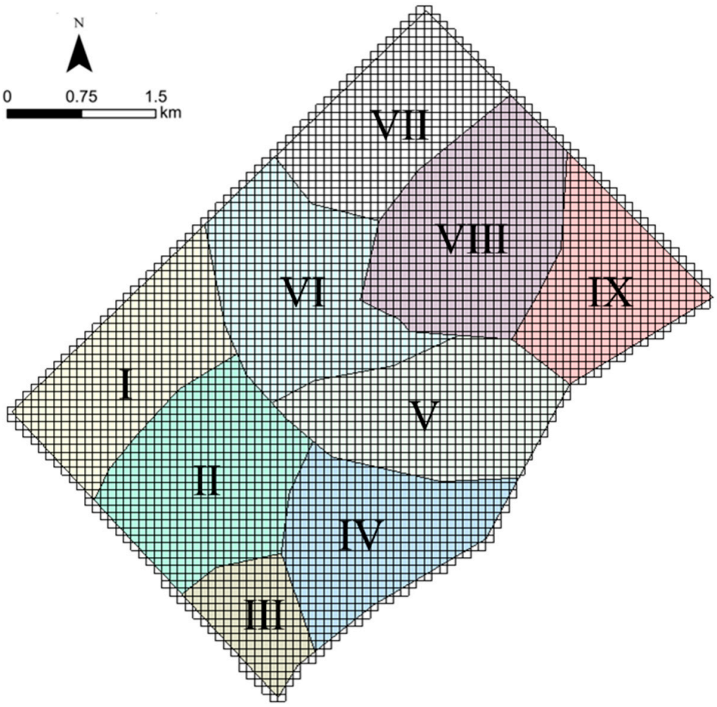

Figure 11. Aquifer parameter zoning (weathered bedrock aquifer).

Table 2. Aquifer parameter zoning table.

Layer	Zone	K_L/m·d^{-1}	K_z/m·d^{-1}	μ	S/m^{-1}
Quaternary Aquifer	I	1.84	0.18	0.12	/
	II	4.61	0.10	0.11	/
	III	1.34	0.13	0.12	/
	IV	2.19	0.12	0.12	/
	V	3.40	0.11	0.12	/
Weathered Bedrock Aquifer	I	0.02	0.02	/	7.5×10^{-4}
	II	0.12	0.15	/	8.5×10^{-4}
	III	0.10	0.29	/	7.5×10^{-4}
	IV	0.03	0.23	/	7.5×10^{-4}
	V	0.22	0.11	/	7.5×10^{-4}
	VI	0.31	0.31	/	6.5×10^{-4}
	VII	0.12	0.26	/	7.5×10^{-4}
	VIII	0.01	0.01	/	7.5×10^{-4}
	IX	0.05	0.02	/	7.5×10^{-4}

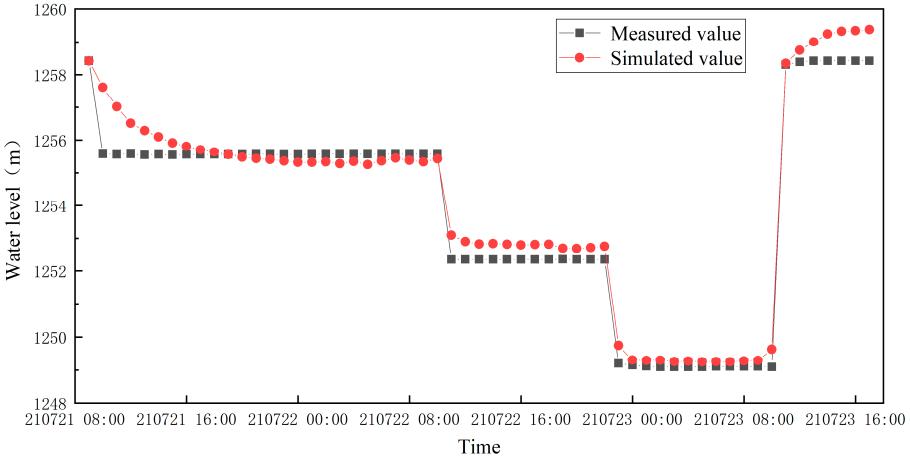

Figure 12. Water level fitting curve of FHS-1 hydropore pumping test.

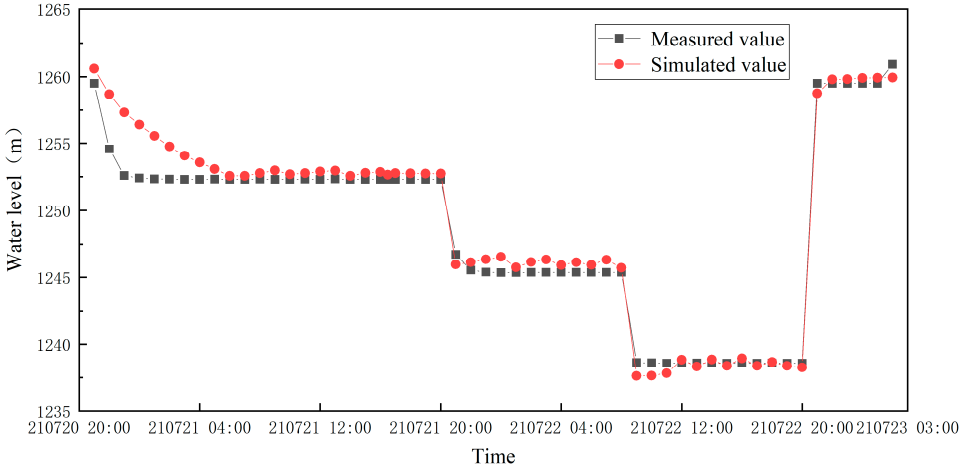

Figure 13. Water level fitting curve of FHS-2 hydropore pumping test.

4.2. Water Inflow Prediction Using GM(1,1)

Based on the water inflow data of the 122107 working face from March to July 2022, the working face water inflow could be predicted by the GM(1,1) model. The results are shown in Table 3.

Table 3. Statistics and forecast results of water inflow at the 122107 working face.

Time	Measured Value/($m^3 \cdot h^{-1}$)	Predicted Value/($m^3 \cdot h^{-1}$)	Error
March 2022	604.8	604.8	0.0%
April 2022	654.7	591.3	9.7%
May 2022	574.5	628.7	9.4%
June 2022	603.7	668.5	10.7%
July 2022	768.4	710.9	7.5%
August 2022		755.9	
September 2022		944.9	
October 2022		1181.1	

Figure 14 shows that there is some discrepancy between the predicted and measured water inflow values. Overall, the degree of coincidence is relatively high, indicating that the model is only a trend prediction. After calculation, the relative error is far less than 20%. Therefore, it can be used as a predictive model.

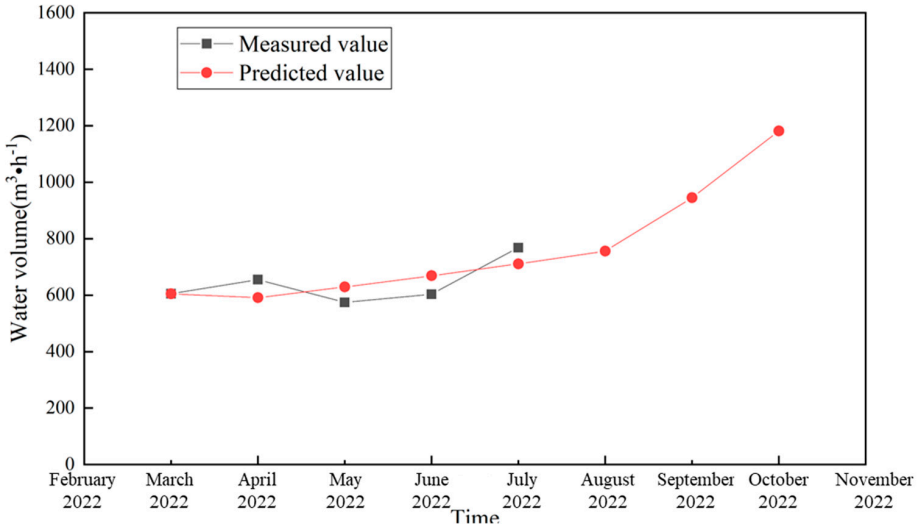

Figure 14. Forecast of mine water inflow.

The average normal water inflow for the months of August, September, and October is 960.6 m^3/h. A value of 1.25 is selected as the maximum water inflow prediction coef-icient for the mine; thus, the maximum water inflow is 1200.8 m^3/h.

4.3. Water Inflow Prediction Using Hydrogeological Analog Method

According to the information provided, the 122109 working face, which is in the western wing of the 12th panel area of the Caojiatan coal mine, uses the Longwall Top Coal Caving mining method, with a mining area of approximately 1.56 km^2. As the adjacent 122107 working face has similar hydrogeological and mining technical conditions, the 122109 working face data are used to predict the water inflow of the 122107 working face. The area of the 122107 working face is approximately 1.80 km^2, and $S = S_0$. In the hydrogeological analogy method, we assume that the hydrogeological conditions of the 122107 working face are similar to those of 122109.

By substituting the selected parameters into Formula (1), the simulation shows that under the condition that the static storage of the water-bearing layer in the roof has been sufficiently pre-drained, the normal water inflow is 923 m^3/h and the maximum water inflow is 1154 m^3/h. As seen in Table 4, S = 526.65 is the depth of water level drop when pumping the aquifer water level down to the bottom of the coal seam, and the values are average values.

Table 4. Parameters for calculation of water inflow using the hydrological analogy method.

Working Face \ Parameter	F (10^6 m^2)	S (m)	Q (m^3/h)
122109	1.56	526.65	800
122107	1.80	526.65	923

4.4. Comparative Validation and Analysis

Table 5 compares the water inflow prediction accuracy for the 122107 working face obtained using various methods with the actual measured water inflow data.

Table 5. List of water inflow prediction results and prediction accuracy of Caojiatan coal mine 122107 working face.

Results \ Data Sources	GM(1,1)	Hydrogeological Analog Method	Numerical Simulation	Measured Value
Normal water inflow Q (m^3/h)	960.6	923	826	807
Maximum water inflowQ (m^3/h)	1200.8	1153.8	1032.5	1008.8
Error (%)	19.0	14.4	2.4	

Through comparison, we find that the results predicted using conventional methods are larger, and the GM(1.1) results vary with the selection of data. The hydrogeological analog method has obvious shortcomings in restoring the actual hydrogeological characteristics of the working face. However, the numerical simulation method overcomes the shortcomings of both.

We find that the prediction results of the numerical simulation method are closer to the measured values upon comparing them with the water inflow observation ledger, and the accuracy is 12–17% higher than that of traditional methods. Therefore, the numerical model is of great significance to study the impacts of deep coal seam mining on the groundwater environment in the northwestern region of China.

5. Conclusions

This paper proposes a method for constructing a mine conceptual hydrogeological model. After fully analyzing the geological characteristics, water sources, water channels,

and water inflow intensity, the model can accurately depict the water inflow process in the 122107 working face of the Caojiatan coal mine.

Based on the mine hydrogeological conceptual model, the numerical simulation is used to finely depict the sharp depositional extinction of the red clay layer, and restore the stratigraphic mine–rock–water structure, the response characteristics of the groundwater system under the conditions of high-intensity coal mining, and the water inflow process, achieving the accurate prediction of water inflow.

Numerical simulation modeling through the mine hydrological conceptual modeling method is able to evaluate the process and intensity of mine water inflow and quantitatively predict the size of mine water inflow. This is a new modeling method to analyze the response characteristics of the groundwater system under high-intensity coal seam mining conditions and to predict the amount of mine water inflow.

In particular, the accuracy of the simulation results is related to the number of hydrological boreholes, and at the same time, the numerical simulation method adopts the average value of a period of time for the prediction of water inflow to the working face instead of the instantaneous inflow, and the water control in coal mines should take the numerical feature into full consideration.

Author Contributions: Z.H., S.M. and Y.Z. (Yao Zhang): conceptualization, methodology, writing—original draft preparation, writing—review and editing, supervision. Y.Z. (Yifan Zeng): conceptualization, supervision, writing—review and editing. L.W., X.W., Y.L., S.R. and J.L.: data curation. H.B., Y.Z. (Yao Zhang), Z.Z. and L.Z.: visualization, investigation. All authors have read and agreed to the published version of the manuscript.

Funding: This research was financially supported by the National Key R&D Program of China (2021YFC2902004) and the China National Natural Science Foundation (42072284, 42372297), Funding Program for Basic Research Operating Expenses of Central Universities (2023ZKPYSH01).

Data Availability Statement: The data presented in this study are available on request from the corresponding author. The data are not publicly available due to [Confidentiality principle].

Conflicts of Interest: The authors declare that they have no known competing financial interest or personal relationships that could have appeared to influence the work reported in this paper.

References

1. Mark, C. Overview of ground control research for underground coal mines in the United States. In Proceedings of the 17th International Mining Congress and Exhibition of Turkey (IMCET 2001), Ankara, Turkey, 19–22 June 2001; pp. 3–10.
2. Dudek, M.; Tajduś, k.; Misa, R.; Sroka, A. Predicting of land surface uplift caused by the flooding of underground coal mines—A case study. *Int. J. Rock Mech. Min. Sci.* **2020**, *132*, 104377. [CrossRef]
3. Zeng, Y.F.; Meng, S.H.; Wu, Q.; Mei, A.S.; Bu, W.Y. Ecological water security impact of large coal base development and its protection. *J. Hydrol.* **2023**, *619*, 129319. [CrossRef]
4. Zhou, S.; Liu, T.; Duan, L. Ecological Impact Prediction of Groundwater Change in Phreatic Aquifer under Multi-Mining Conditions. *ISPRS Int. J. Geo Inf.* **2022**, *11*, 359. [CrossRef]
5. Li, B.; Zeng, Y.F.; Zhang, B.B.; Wang, X.Q.; Risk, A. Evaluation Model for Karst Groundwater Pollution Based on Geographic Information System and Artificial Neural Network Applications. *Environ. Earth Sci.* **2018**, *77*, 344.
6. Bicalho, C.C.; Batiot-Guilhe, C.; Taupin, J.D.; Patris, N.; Van Exter, S.; Jourde, H. A Conceptual Model for Groundwater Circulation Using Isotopes and Geochemical Tracers Coupled with Hydrodynamics: A Case Study of the Lez Karst System, France. *Chem. Geol.* **2019**, *528*, 118442. [CrossRef]
7. Lu, C.Y.; He, X.; Zhang, B.; Wang, J.H.; Kidmose, J.; Jarsjö, J. Comparison of Numerical Methods in Simulating Lake–Groundwater Interactions: Lake Hampen, Western Denmark. *Water* **2022**, *14*, 3054. [CrossRef]
8. Zeng, Y.F.; Wu, Q.; Liu, S.Q.; Zhai, Y.L.; Lian, H.Q.; Zhang, W. Evaluation of a Coal Seam Roof Water Inrush: Case Study in the Wangjialing Coal Mine, China. *Mine Water Environ.* **2018**, *37*, 174–184. [CrossRef]
9. Zeng, Y.F.; Li, Z.; Gong, H.J.; Zheng, J.H. Characteristics of Water Abundance in the Aquifer of Weathered Bedrock of 2-2 Coal Roof in Ningtiaota Coal Mine and Prediction on Water Inrush Risk. *Coal Eng.* **2018**, *50*, 100–104.
10. Zeng, Y.F.; Wu, Q.; Liu, S.Q.; Zhai, Y.L.; Zhang, W.; Liu, Y.Z. Vulnerability Assessment of Water Bursting from Ordovician Limestone into Coal Mines of China. *Environ. Earth Sci.* **2016**, *75*, 1431. [CrossRef]
11. Ta, D.; Cao, S.; Steyl, G.; Yang, H.Y.; Li, Y. Prediction of Groundwater Inflow into an Iron Mine: A Case Study of the Thach Khe Iron Mine, Vietnam. *Mine Water Environ.* **2019**, *38*, 310–324. [CrossRef]
12. Duan, L.; Wang, W.K. Water Lsotope Technology for Tracing Groundwater Movement. *Ground Water* **2006**, *2*, 33–36.

13. Wu, Q.; Tu, K.; Zeng, Y.F. Research on China's energy strategic situation under the carbon peaking and carbon neutrality goals. *Chin. Sci. Bull.* **2023**, *68*, 1884–1898. [CrossRef]
14. Wu, Q.; Tu, K.; Zeng, Y.F.; Liu, S.Q. Discussion on the main problems and countermeasures for building an upgrade version of main energy (coal) industry in China. *J. China Coal Soc.* **2019**, *44*, 1625–1636.
15. Li, W.J.; Ren, S.L.; Wu, Q.; Dong, D.L.; Gan, X.Y. Analysis on the dual constraints of energy and environment to the development of China and countermeasures. *Chin. Sci. Bull.* **2019**, *64*, 1535–1544.
16. Wu, C.; Wu, X.; Zhu, G.; Qian, C. Predicting Mine Water Inflow and Groundwater Levels for Coal Mining Operations in the Pangpangta Coalfield, China. *Environ. Earth Sci.* **2019**, *78*, 130. [CrossRef]
17. Zeng, Y.F.; Meng, S.H.; Lü, Y. Advanced Drainage Technology Based on Multi-objective Constraint of Mine Safety and Water Resources Protection. *J. China Coal Soc.* **2022**, *47*, 3091–3100.
18. Chen, S. Mine Water Inrush Prediction Based on Virtual Large Diameter Well Method. *IOP Conf. Ser. Earth Environ. Sci.* **2019**, *300*, 022098.
19. Liu, H.R.; Yan, Y.F.; Yang, H.T. The Prediction of the Water Yield Which Flood from the Pit and the Trait of the Hydrogeology Which Existed in the Mining Area of the Zhujiabaobao Mining in Panzhihua. *Appl. Mech. Mater.* **2013**, *401*, 2155. [CrossRef]
20. Ling, H.; Wang, L.X. A Study on Water Filling Factors and Inflow Prediction in Malin Coal Mine Extended Mining Sector, Lupanshui Mining Area. *Coal Geol. China* **2017**, *29*, 53–56.
21. Mi, J.K.; Wang, T. Application of Analytic Method on Working Face Water Lnflow Prediction in Xinglongzhuang Coal Mine. *Coal Geol. China* **2011**, *23*, 27–30.
22. Wang, F.L. Study on Optimization of Mine Water Inflow Calculation Methods in Different Production Periods. *Coal Sci. Technol.* **2019**, *47*, 177.
23. Luo, Z.J.; Zhao, L.I.; Ren, H.-J. Numerical Simulation Research on Prediction of Mine Inflow. *Coal Sci. Technol.* **2015**, *43*, 33–36.
24. Zhang, B.J. Mine Water Inflow Forecast Based on Visual Modflow in Taigemiao Exploration Area. *Coal Sci. Technol.* **2015**, *43*, 146.
25. Pang, Y.; Li, S.Y. Simulation Prediction of Mine Water Surges Based on Visual MODFLOW. *Sci. Res. Rev.* **2022**, *15*, 126.
26. Wang, G.R.; Wu, Q.; Yan, Z.Z.; Zhao, N.; Duan, C.B.; Cheng, X.; Wang, H. Fine Prediction for Mine Water Inflow on Basis of Visual Modflow. *Int. J. Oil Gas Coal Eng.* **2019**, *7*, 52–59.
27. Bayat, M.; Eslamian, S.; Shams, G.; Hajiannia, A. Groundwater Level Prediction Through GMS Software—Case Study of Karvan Area, Iran. *Quaest. Geogr.* **2020**, *39*, 139–145. [CrossRef]
28. Hu, X.J.; Ling, W.P.; Cao, D.T.; Liu, M.C. Index of Multiple Factors and Expected Height of Fully Mechanized Water Flowing Fractured Zone. *J. China Coal Soc.* **2012**, *37*, 613–620.
29. Zhong, H.; Qu, G.R.; Huang, L.X. Quantitative Simulation of Groundwater by Mathematical Model in Muzhu River Aquifer Using GMS. *IOP Conf. Ser. Earth Environ. Sci.* **2020**, *510*, 042020.
30. Ni, L.D.; Fan, M.Y.; Qu, S.S.; Zheng, Q.Y. Based on GMS Management of Shallow Groundwater Resource in Ningjin, China. *IOP Conf. Ser. Earth Environ. Sci.* **2019**, *237*, 032063. [CrossRef]
31. Liang, Y.M.; Lan, J.K.; Wen, Z.X. Simulation and Prediction of Groundwater Pollution from Planned Feed Additive Project in Nanning City Based on GMS Model. *IOP Conf. Ser. Earth Environ. Sci.* **2018**, *301*, 012159. [CrossRef]
32. Chen, M.J.; Izady, A.; Abdalla, O.A. An Efficient Surrogate-Based Simulation-Optimization Method for Calibrating a Regional MODFLOW Model. *Hydrology* **2017**, *544*, 591–603. [CrossRef]
33. Bo, Q.Y.; Cheng, W.Q.; Sun, T. Groundwater Simulation Model for Baohe River in the Upper Reaches of Baiyangdian Lake Based on Groundwater Simulation Software (GMS). *J. Environ. Prot. Ecol.* **2021**, *22*, 1162–1174.
34. Sartirana, D.; Zanotti, C.; Rotiroti, M.; De Amicis, M.; Caschetto, M.; Redaelli, A.; Fumagalli, L.; Bonomi, T. Quantifying Groundwater Infiltrations into Subway Lines and Underground Car Parks Using MODFLOW-USG. *Water* **2022**, *14*, 4130. [CrossRef]
35. Li, Q. The Grey Elementary Functions and Their Grey Derived Functions. *J. Grey Syst.* **2008**, *20*, 225–245.
36. Islam, M.R.; Kabir, G.; Ng, K.T.W.; Ali, S.M. Yard Waste Prediction from Estimated Municipal Solid Waste Using the Grey Theory to Achieve a Zero-Waste Strategy. *Environ. Sci. Pollut. Res. Int.* **2022**, *29*, 46859. [CrossRef] [PubMed]
37. Wei, W.D.; Wang, G.; Tao, X.; Luo, Q.; Chen, L.X.; Bao, X.L.; Liu, Y.X.; Jiang, J.J.; Liang, H.; Ye, L. Time Series Prediction for the Epidemic Trends of Monkeypox Using the Arima, Exponential Smoothing, GM (1, 1) and LSTM Deep Learning Methods. *J. Gen. Virol.* **2023**, *104*, 001839. [CrossRef]
38. Cao, J.M.; Chi, B.M.; Wang, W.K. *Specialized Hydrogeology*; China Science Publishing: Beijing, China, 2006; pp. 226–241.
39. Xu, N.W.; Dai, F.; Li, B.; Zhu, Y.G.; Zhao, T.; Yang, D.S. Comprehensive Evaluation of Excavation-Damaged Zones in the Deep Underground Caverns of the Houziyan Hydropower Station, Southwest China. *Bull. Eng. Geol. Environ.* **2017**, *76*, 275–293. [CrossRef]
40. Qu, H.; Liu, H.; Tan, K.; Zhang, Q. Geological Feature Modeling and Reserve Estimation of Uranium Deposits Based on Mul-Tiple Interpolation Methods. *Processes* **2022**, *10*, 67. [CrossRef]